Journal of Power Sources 239 (2013) 500–504

Contents lists available at SciVerse ScienceDirect

Journal of Power Sources

journal homepage: www.elsevier.com/locate/jpowsour

Short communication

Elevated temperature effects on the mechanical properties of solid oxide fuel cell sealing materials

Yilin Zhao, Jürgen Malzbender*

Forschungzentrum Jülich GmbH, IEK-2, 52425 Jülich, Germany

HIGHLIGHTS

- Partially crystallized sealants showed viscous effects above T_g (~700 °C)
- Partially crystallized sealants had drop in elastic modulus and strength above T_g.
- Fully crystallized material shows stable properties (T_g ~900 °C).
- Polishing increases the fracture stress by 30%.
- Critical flaw size is a factor of ~10 larger for partially crystallized material.

ARTICLE INFO

Article history:
Received 24 July 2012
Received in revised form
22 March 2013
Accepted 7 April 2013
Available online 19 April 2013

Keywords:
Solid oxide fuel cells
Sealant
Mechanical properties
Fracture
Viscosity

ABSTRACT

A promising candidate to fulfil the solid oxide fuel cell sealant requirements with respect to gas tightness, high temperature stability and electrical insulation appear to be glass-ceramic sealing materials. However, the reliable operation of solid oxide fuel cell stacks depends strongly on the structural integrity of the sealing materials. In this respect failure and deformation are aspects which need to be assessed in particular for glass ceramic sealant materials. Bending tests were carried at room temperature and typical stack operation temperature for glass ceramic sealants with different degree of crystallization. Elastic moduli, fracture stresses and viscosity values are reported. In addition to sintered bars bending testing were carried out for steel specimens that were head-to-head joined with the glass ceramics similar as in a stack application, where the ceramic particle reinforced sealant material was screen printed onto the steel. The results reveal a decrease of the strength for the partially crystallized sealant at operation relevant temperatures that can be associated with the viscous deformation. Fractographic analyses based on a combination of optical, confocal and scanning electron microscopy gave insight into the failure origin.

© 2013 Elsevier B.V. All rights reserved.

1. Introduction

The reliability and robustness of sealants are a prerequisite for the commercialization of planar solid oxide fuel cells (SOFCs). Approaches to join and seal stacks have been based on glasses, glass-ceramics, glass-composites and metallic materials [1–4]. The sealant should separate anode and cathode gas compartment hermetically and not show any unwanted chemical interactions to other component materials or gaseous species and furthermore, possess a sufficient bonding strength to withstand operation induced stresses. Glasses and glass-ceramics have better resistance to the oxidizing and reducing atmospheric in the stack than metallic sealants and appear to fulfil most SOFC specific requirements. Glass-ceramics are cheaper than related metallic sealing materials and can be applied to the sealing surfaces as a powder dispersed in a paste, as tape casted sheets or by screen printing. Furthermore, they typically exhibit better wetting behaviour than metallic sealants, are electrically insulating and can be engineered to exhibit similar coefficient of thermal expansion (CTE) as the adjacent SOFC components, thereby minimizing thermally induced stresses [2,5]. Another most important criterion for the sealant design and development is the glass transition temperature T_g, above which the materials behaviour changes from brittle to ductile [6,7]. Viscous stress relaxation or occurrence of structural instabilities coupled with strength reduction might be expected above T_g.

During the joining process, the initial glass might partially or fully crystallize and react with the metallic interconnect materials

* Corresponding author. Tel.: +49 2461 616964; fax: +49 2461 613699.
E-mail address: j.malzbender@fz-juelich.de (J. Malzbender).

0378-7753/$ – see front matter © 2013 Elsevier B.V. All rights reserved.
http://dx.doi.org/10.1016/j.jpowsour.2013.04.043

or any existing oxide layer. The resulting interaction phases might thicken with increasing operation times and become porous, yielding weak interfaces that can be susceptible to thermo-mechanically induced cracking [8,9]. The crystallized materials are typically mechanically stronger. However the final joint can expect to be brittle and fracture susceptible when exposed to tensile stresses that might result of components CTE mismatches or simply thermal cycling operation induced temperature gradients [8]. As an alternative to fully crystallized glass-ceramics, particle or fibre reinforcements might be considered as means to optimize the fracture toughness by crack stopping and deflection mechanism [10,11]. A brittle filler material with high elastic modulus and toughness can dissipates energy during pull out or by a change in crack path.

In the present work, results of the mechanical characterization of two glass-ceramic sealants are reported. One ceramic filler particle reinforced sealant with a rather low level of crystallization (abbreviated H, 80% glassy phase) and one without reinforcement which is almost fully crystallized (B, <10% glassy phase). The materials are characterized with respect to elastic and viscous behaviour, and strength. Tests are carried out for sintered bars or in a head-to-head joined geometry.

2. Experimental

The partially crystallized glass-ceramic sealant (H) was based on a glass matrix of the BaO–CaO–SiO_2 ternary system with addition of small amounts of Al_2O_3, B_2O_3, V_2O_5, and ZnO [12]. The raw materials were obtained from Merck KGaA, Darmstadt and had a purity grade higher than 99%. Each batch was prepared by mixing an appropriate mole fraction of oxide ingredients and melting at 1480 °C in an induction furnace in a platinum crucible [3]. For a better homogenization, the melting procedure was carried out twice. For subsequent powder preparation, the frits were wet-milled in acetone in an agate ball mill to a median particle size of 10–13 μm, dried and then sieved through a 32 μm size mesh. The chemical composition of the material was analyzed by inductively coupled plasma optical emission spectroscopy (ICP-OES) yielding BaO – 48.2, SiO_2 – 29.8, and CaO – 6.1 wt.% with minor additions of Al_2O_3, B_2O_3, V_2O_5, and ZnO. To obtain sintered rods, a conventional sintering process was carried out, powders were mixed with YSZ particles (sizes 1–40 μm) and pressed and sintered on a wavelike curved platinum foil at 850 °C for 10 h and then cooled down to room temperature (RT). Heating and cooling rates were 5 K min^{-1}.

The almost fully crystallized glass-ceramic sealant (B) is also based on BaO–CaO–SiO_2 system, however with addition of only Al_2O_3 and received otherwise the same processing as the H series [12]. Chemical composition of the material was also analyzed by ICP-OES, yielding a composition of BaO – 36.7, SiO_2 – 46.8, and CaO – 15.8 wt.%, with minor additions of Al_2O_3. The powder was pressed and sintered at 950 °C for 10 h. Heating and cooling rate was also 5 K min^{-1}.

The head-to-head joined specimens were prepared using an in-house developed sealing jig [13]. Similar as in SOFC stacks [8], Crofer22APU was used as steel for the joint, with a surface preparation equivalent to that typical for stack application. The sealant was deposited by screen printing. Specimens dimensions were 52 mm × 6 mm × 4 mm with a sealant thickness of <0.2 mm. The uncertainty for dimensions and parallelism for head-to-head joined specimens and sintered bars was 0.05 mm.

Five specimens of each variation were tested in four-point bending in the as-joined state and after additional polishing of either the tensile side or of all sealant surfaces. The fracture stress of the head-to-head joined specimens was determined after ASTM C1161[see also [14–16]. In addition viscous deformation was investigated in bending tests for bars and head-to-head joined specimens. The viscous bending rupture was investigated only for material H (3 specimens) in the as-joined state at typical operation temperatures. The tests were carried out up to failure at 800 °C in air with the heating rate of 5 K min^{-1}. The viscosity was determined as outlined in Ref. [13]. The elastic modulus of the sintered bars was determined using impulse excitation (Grindosonic, Lemens KG, Belgium).

3. Results and discussion

The CTE of material B [17] and H (non-aged and aged) [18] (non-aged and aged) are compared in Fig. 1 to the values of the interconnect steel Crofer22APU and the NiO/YSZ anode substrate [18]. The CTE has been determined for sintered bars; experimental details are given in Refs. [17,18]. The CTE of sealant H in the glassy state shows a strong increase when the glass transition state (T_g) of about 640 °C is approached. The softening temperature (T_s) of ~750 °C can be seen as peak of the CTE curve. The obtained glass transition temperature for material B is ~700 °C. Overall the values are higher than for H material. The softening is observed around the same temperature. Details on the crystallization temperature (differential thermal analysis), softening temperature ("sinking dilatometer") [19] and transformation temperature (dilatometer) can be found in Ref. [18]. Since the CTE of glass-ceramic H is smaller than that of metallic parts and cermet, compressive stresses are induced into the material on cooling, which is advantageous for ceramic materials. It has been verified in numerous stack tests [8] that the sealant survives stack operation and moderate thermal cycling and that in fact in the case of thermal cycling stresses generated by in-plane temperature gradients that are not related to CTE differences appear to be the main problem [8].

For the stack typical as-joined state (Fig. 2), it might be suggested on the basis of the curves in Fig. 1 that the glass transition temperature is reduced to about 600 °C for sealant H. Such reductions in the transition temperature associated with a different composition of the remaining glassy matrix after the crystallization process have been discussed in Ref. [20]. It has been suggested that when the concentration of crystalline phases is low, the cross-linking density of the remaining glass will decrease, resulting in a decrease of the glass transition temperature [20]. Sealant B

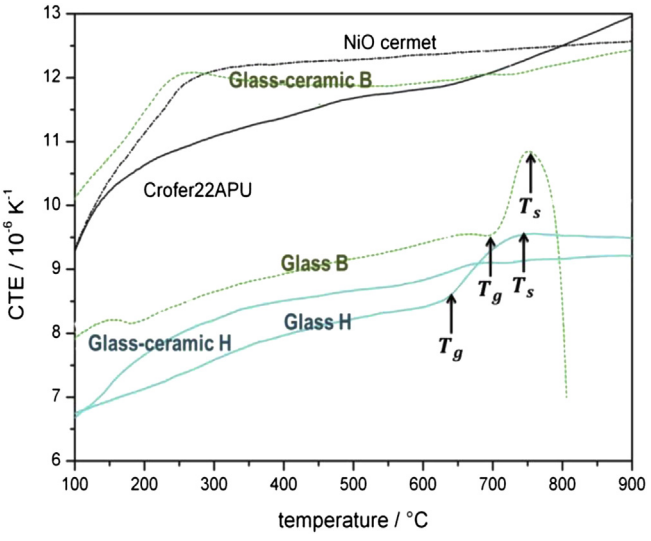

Fig. 1. CTE of material B and H in the glassy and crystallized state.

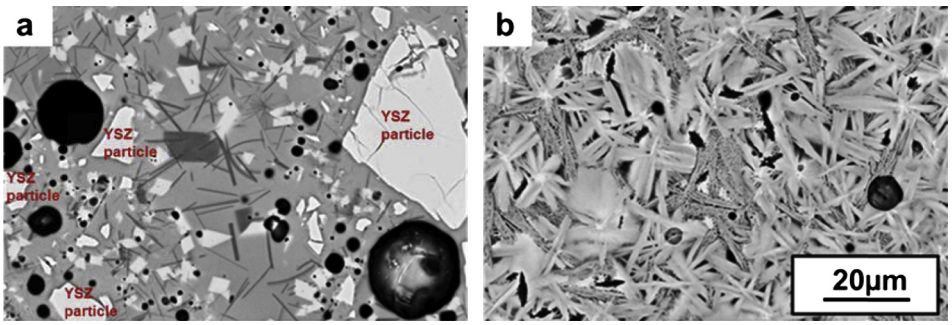

Fig. 2. Microstructural image obtained using SEM of as-joined sealant (a) H and (b) B.

Table 1
Average fracture stress in MPa.

Material/temperature			Room temperature	800 °C
H	Head-to-head joined	Unpolished	43 ± 1	×
		Polished	52 ± 1	~1 [13]
	Bar		55 ± 7 [13]	10 ± 2 [13]
B	Bar		91 ± 12 [13]	~90 [13]

(porosity less than 1%) did not display any indications of a transition or softening temperature up to 900 °C as a result of the almost fully crystallized state of the material (Fig. 2). For a typical stack operation temperature the CTE of the as-joined state of sealant H is close to 9.5 × 10^{-6} K^{-1}, for the sealant B close to 12 × 10^{-6} K^{-1}.

The SEM image of the material H (local porosity about 10%–40%, average porosity ~20%) in Fig. 2 a shows white flakes of binary barium silicates. The dark grey bars are barium alumino-silicates, which appear to be the main crystalline phase, while the grey regions reflect the residual glass [21]. The big white structures are the YSZ particles added as reinforcement. In addition some micro-pores can be seen. It has been shown that the sealants contain micro- and macro-pores (see also Fig. 7 below) resulting from volume shrinkage associated with the crystallization process [18]. The micro-cracks in the large YSZ particle is a result of the specimens preparation. In spite of the large interfacial areas, the glass nucleation and crystallization appears not to be influenced by the YSZ particles [21]. The deflection of cracks by these particles has been verified in Refs. [21], where it was also shown that the fracture toughness of the material is improved by the particles.

The impulse excitation obtained elastic modulus of the as-joined sealant B revealed a ~10% decrease between RT and

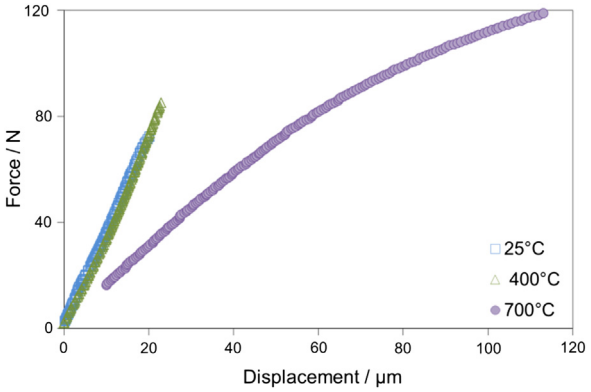

Fig. 3. Force-displacement curves for head-to-head jointed H (loading rate 0.6 MPa s^{-1}).

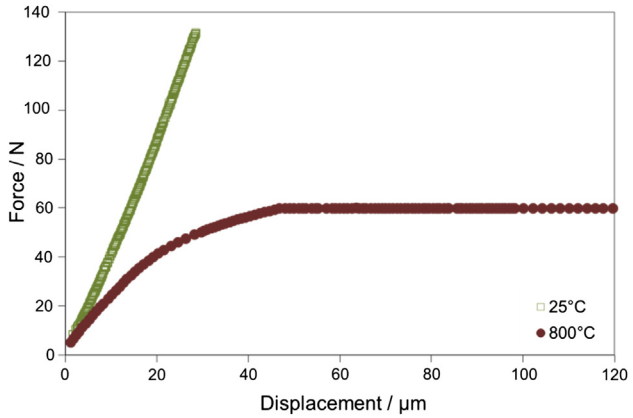

Fig. 4. Force-displacement curves for head-to-head jointed B (loading rate 0.6 MPa s^{-1}).

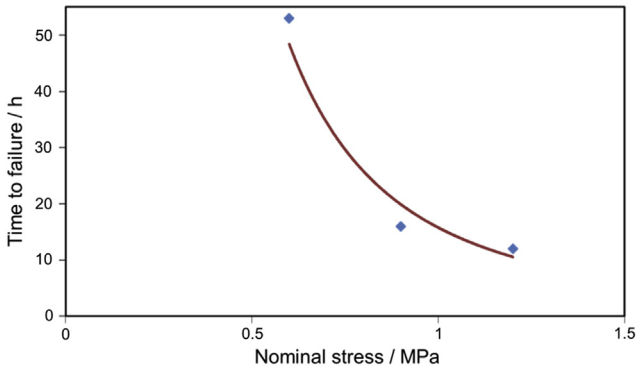

Fig. 5. Rupture time as a function of nominal applied stress for head-to-head jointed H.

800 °C [13]. The apparent elastic modulus of glass-ceramic H decreased similarly by ~10% from RT to 650 °C, however, dropped strongly above this temperature due to softening of the glassy matrix. In fact, the RT elastic moduli of ~82 GPa for glass-ceramic B

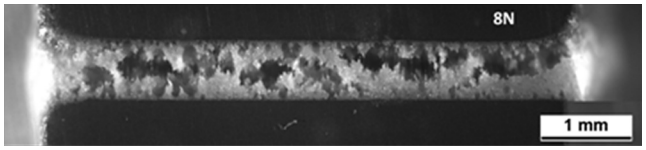

Fig. 6. Stereo-microscopic image of a head-to-head joined specimen of material H after rupture test (1.2 MPa at 700 °C).

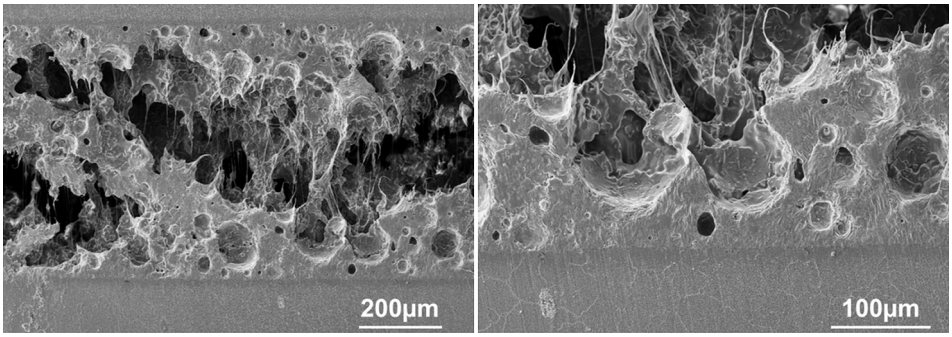

Fig. 7. SEM images of a head-to-head joined H type specimen (1.2 MPa at 700 °C).

and ~76 GPa for H agreed with the values obtained using indentation testing [21]. The rather large uncertainty (~10–15 GPa) observed in indentation tests for glass-ceramic H associated with the high porosity was not reflected in the impulse excitation measurement. In general a decrease of average modulus due to the rather large porosity of the material can be expected. An estimate based on [22] leads to a factor ~ two higher elastic modulus for the dense state of material H.

A recently developed joining jig permitted to measure the fracture stress for sealant H in stack typical layer geometry on the basis of four-point bending tests of head-to-head joined specimens in Table 1. The thickness of the glass-ceramic layer as determined using optical microscopy was between 45 and 80 µm. The average fracture stress of 43 ± 1 MPa for unpolished specimens increased to 51 ± 6 and 52 ± 1 MPa for specimens with either the tensile or all surfaces polished before the test. For all specimens cohesive failure was observed without indications of interfacial delamination. The lower strength for the unpolished material can be a result of stress concentration due to the joining angle that resulted from wetting limitations [23]. The results for polished head-to-head joined specimens are in good agreement with the average fracture stress reported for sintered polished bars [13]. Although the data for sintered bars and polished head-to-head joined specimen represent the fracture strength of the material, the data for the unpolished head-to-head joined specimens are more representative for the failure situation in the SOFC stack, where the notch effect also leads to a stress concentration and thereby a reduction of the apparent fracture stress.

Although the sealant will be at RT under the highest stress due to the CTE mismatch with the adjacent components, also the non-elastic properties at operation relevant temperatures should receive consideration since they affect the long-term reliability. To assess the strength at elevated temperatures a limited number of four-point bending tests have been carried out at 800 °C with sintered bars, revealing a decrease of the average fracture stress for sealant H to 10 ± 2 MPa, whereas the fully crystallized sealant type B showed no strength decrease [13]. Tests at elevated temperatures with head-to-head joined specimens of type H turned out to be only of limited success since the specimens failed under the experimentally necessary preload (~1 MPa) already during heating below 800 °C. The specimen already deformed during heating, which led to an accumulated strain and subsequently decreased the apparent fracture stress at 800 °C [13].

The critical flaw size was estimated using a Griffith criterion. The RT fracture toughness values reported in Ref. [24] yield for sealant H a critical flaw size of ~100 µm and for the almost fully crystallized variant B a value of ~10 µm, which corresponds well to pores observed for this material (Fig. 2). Since it is reasonable to assume that the critical defect size is temperature independent, the lower fracture stress at elevated temperatures for sealant H suggests a lower high temperature fracture toughness (due to lower elastic modulus and/or fracture energy).

The bending test force-displacement curves obtained at different temperatures for the head-to-head jointed variant H are shown in Fig. 3 (loading rate 0.6 MPa s^{-1}). The curves were linear below 700 °C. The non-linearity at 700 °C suggests an influence by viscous effects [25], in agreement with the observed softening effects in CTE and elastic modulus.

A similar test on the effect of viscous deformations has been carried out for head-to-head jointed specimens for material B. Due to the rather low loading rate and the holding time introduced at a maximum load of 60 N, non-elastic deformation of 6 µmh^{-1} became clearly visible at 800 °C (Fig. 4), verifying that this fully crystallized material still has stress relaxation potential. For sintered sealant H bars tests have been carried out under constant load in a three-point bending arrangement at 800 °C. The resulting viscosity as obtained was ~3 × 10^9 dPa s in agreement with the average viscosity of head-to-head joined specimens for a temperature range of 700–800 °C. A much higher value of ~400 × 10^{12} dPa s has been obtained for the fully crystallized glass-ceramic of type B.

In an attempt to predict the long-term reliability of the material the time to failure at elevated temperatures has been determined on the basis of four-point bending tests at 700 °C for the head-to-head joined sealant material H in air under constant applied stress 0.6, 0.9 and 1.2 MPa, respectively. It appears that viscous deformation leads to non-linear stress strain behaviour and eventually rupture. The resulting viscous rupture times versus the nominal applied stress are presented in Fig. 5. The data imply that the time to viscous failure is approximately inverse proportional to the squared applied nominal stress. Unless a threshold exists, even low tensile stresses will lead to failure. For example it can be extrapolated that in a bending equivalent situation the sealant will only survive a stack operation time of 40,000 h for a stress level below 0.03 MPa.

The ruptured specimens were analyzed using stereomicroscopy (Fig. 6) and SEM (Fig. 7) in order to get insight into the microstructural failure mechanisms. The images imply that the failure is associated with smaller opening in the glassy matrix which increases in size with time. It appears that these openings in the matrix initiate at the edges of big pores inside the glassy layer (Fig. 7). Then they grow in direction of the stress field and eventually join with others to form the macroscopic rupture. Hence the viscous flow of the glassy phase has the potential to lead eventually to the observed failure above the glass transition temperature (~600 °C for the as-joined state).

4. Conclusion

Due to the high reliability requirements for planar SOFC stacks, the mechanical properties of sealants materials have to receive

considerable attention. In addition to results on elastic and non-elastic deformation behaviour, also failure data have been presented for one partially and one almost fully crystallized glass ceramic sealant material for room temperature and typical stack operation temperatures, yielding elastic moduli, viscosity and fracture stress data, respectively. The results reveal a decrease of the strength at operation relevant temperatures for the partially crystallized material due to viscous deformation. The almost fully crystallized material exhibits no measureable strength decrease at elevated temperatures and in addition a higher viscosity. The viscous rupture of the partially crystallized sealant has been investigated yielding details of the failure mechanism and rupture times for different nominal applied stresses that can be used to estimated lifetimes.

Acknowledgements

The authors would like to express their gratitude to Dr. S. M. Groß who designed, developed and made available the sealant material for the mechanical tests, Mr. D. Federmann for the screen printing of the material and to Dr. D. Grüner for the SEM investigations. The experimental support by Ms. T. Osipova and Mr. J. Mönch is highly appreciated.

References

[1] F. Smeacetto, M. Salvo, F.D. D'Hérin Bytner, P. Leone, M. Ferraris, J. Eur. Ceram. Soc. 30 (2009) 933–940.
[2] M.K. Mahapatra, K. Lu, Mater. Sci. Eng. R 67 (2010) 65–85.
[3] S.-M. Gross, T. Koppitz, J. Remmel, U. Reisgen, Ceram. Eng. Sci. Proc. 26 (4) (2005) 239.
[4] B. Kuhn, E. Wessel, J. Malzbender, R.W. Steinbrech, L. Singheiser, Int. J. Hydrogen Energy 35 (2010) 9158–9165.
[5] S. Ghosh, P. Kundu, A. Das Sharma, R.N. Basu, J. Eur. Ceram. Soc. 28 (2008) 69–76.
[6] J. Malzbender, R.W. Steinbrech, J. Power Sources 173 (2007) 60–67.
[7] D. Bahadur, N. Lahl, K. Singh, L. Singheiser, K. Hilpert, J. Electrochem. Soc. 151 (2004) A558–A562.
[8] L. Blum, S.M. Groß, J. Malzbender, U. Pabst, M. Peksen, R. Peters, I.C. Vinke, J. Power Sources 196 (2011) 7175–7181.
[9] K.D. Meinhardt, D.-S. Kim, Y.-S. Chou, K.S. Weil, J. Power Sources 182 (2008) 188–196.
[10] M.D. Thouless, O. Sbaizero, L.S. Sigl, A.G. Evans, J. Am. Ceram. Soc. 72 (1989) 525–532.
[11] D.B. Marshall, A.G. Evans, J. Am. Ceram. Soc. 68 (1985) 225–231.
[12] S.M. Gross, D. Federmann, J. Remmel, M. Pap, J. Power Sources 196 (2011) 7338–7342.
[13] J. Malzbender, Y. Zhao, Fuel Cells (2012) 47–53.
[14] J. Malzbender, R.W. Steinbrech, L. Singheiser, CESP 26 (2005) 293–298.
[15] J. Malzbender, R.W. Steinbrech, J. Eur. Ceram. Soc. 27 (2007) 2597–2603.
[16] J. Malzbender, R.W. Steinbrech, J. Eur. Ceram. Soc. 28 (2008) 247–252.
[17] J. Malzbender, T. Koppitz, S.M. Gross, R.W. Steinbrech, in: Proceedings of the 7th European SOFC Forum (2006) P0418.
[18] S.M. Gross, U. Reisgen, Schweißen und Schneiden 59 (2007) 70–77.
[19] M.S. Reichle, T. Koppitz, D. Federmann, U. Reisgen, Materialwiss. Werkstofftech. 42 (2011) 188–199.
[20] R. Hill, P. Gilbert, J. Am. Ceram. Soc. 76 (1993) 417–425.
[21] Y. Zhao, J. Malzbender, S.M. Gross, J. Eur. Ceram. Soc. 31 (2011) 541–548.
[22] B.X. Huang, V. Vasechko, Q.L. Ma, J. Malzbender, J. Power Sources 206 (2012) 204–209.
[23] A. Müller, S. Goswami, J. Hohe, W. Becker, Proc. Appl. Math. Mech. 4 (2004) 288–289.
[24] J. Malzbender, Y. Zhao, J. Mater. Sci. 47 (2012) 4342–4347.
[25] H.-T. Chang, C.-K. Lin, C.-K. Liu, J. Power Sources 189 (2009) 1093–1099.